Direct-Writing of Cu Nano-Patterns with an Electron Beam

Shih-En Lai,[a] Ying-Jhan Hong,[a] Yu-Ting Chen, Yu-Ting Kang, Pin Chang, and Tri-Rung Yew[*]

Department of Materials Science and Engineering, National Tsing-Hua University, Hsinchu 30013, Taiwan, R.O.C.

Abstract: We demonstrate direct electron beam writing of a nano-scale Cu pattern on a surface with a thin aqueous layer of $CuSO_4$ solution. Electron beams are highly maneuverable down to nano-scales. Aqueous solutions facilitate a plentiful metal ion supply for practical industrial applications, which may require continued reliable writing of sophisticated patterns. A thin aqueous layer on a surface helps to confine the writing on the surface. For this demonstration, liquid sample holder (K-kit) for transmission electron microscope (TEM) was employed to form a sealed space in a TEM. The aqueous $CuSO_4$ solution inside the sample holder was allowed to partially dry until a uniform thin layer was left on the surface. The electron beam thus reduced Cu ions in the solution to form the desired patterns. Furthermore, the influence of e-beam exposure time and $CuSO_{4(aq)}$ concentration on the Cu reduction was studied in this work. Two growth stages of Cu were shown in the plot of Cu thickness versus e-beam exposure time. The measured Cu reduction rate was found to be proportional to the $CuSO_{4(aq)}$ concentration.

Key words: electron beam-induced deposition, direct writing, Cu pattern, liquid cell, electron microscopy

INTRODUCTION

Nano-scale metal patterns play a key role in biology, chemistry, engineering, and physics with applications including Cu interconnects in integrated circuit chips, Au nanodot arrays in surface plasmon resonance biosensors (Vazquez-Mena et al., 2011), Ag nanowire networks in transparent conducting electrodes (De et al., 2009; van de Groep et al., 2012), and ring-shaped metals in split-ring resonators (Shelby et al., 2001; Smith et al., 2004).

Extensive research has been done on various direct-writing technologies for Cu patterns. Direct-writing is a prospective technology where maskless patterning is required. Utke et al. (2002), Ochiai (1996), and Friedli et al. (2009) used an electron beam (e-beam) to reduce Cu from Cu-containing gas precursors, $C_5O_2HF_6$-Cu(I)-C_5H_{12}Si and $Cu(C_5HF_6O_2)_2$. With the high convergence and controllability of an e-beam, Cu lines with a width of 200 nm were produced. Manshina et al. (2007) reduced Cu from a $CuCl_2$ solution with a laser beam. $CuCl_2$ solution is nontoxic and low-cost compared with $C_5O_2HF_6$-Cu(I)-C_5H_{12}Si. Nevertheless, the width of the Cu line was roughly at the micrometer scale limited by laser beam size. In this work, we focused on producing nano-scale Cu with a simple and low-cost process. Direct-writing of Cu nano-patterns with an e-beam on a surface in a uniform and stable thin aqueous layer was demonstrated.

The concept of this work is shown in Figure 1a. A copper sulfate ($CuSO_4$) solution formed a thin liquid layer

on top of the substrate and an e-beam was utilized to reduce Cu from the solution. In practical applications, Cu patterns can be obtained by first applying a $CuSO_4$ solution on a substrate such as a silicon wafer and then manipulating an e-beam with a predesigned path to reduce Cu from the solution. Recently a similar concept was reported by some groups (Randolph et al., 2013; Bresin et al., 2014; den Heijer et al., 2014). Randolph et al. (2013) and Bresin et al. (2014) applied the $CuSO_4$ solution on a Si wafer and Cu reduction was conducted in an environmental scanning electron microscope (ESEM). Temperature of the Si wafer and pressure of the ESEM were then used to control the solution's saturation vapor pressure to prevent evaporation. The radius of the solution droplet was around $100 \mu m$. The droplet, with the cohesive force of water, formed a bow-shape on a Si wafer, which resulted in a different incident path of the e-beam and influenced uniformity of the reduced Cu. Therefore, a uniform and stable liquid thin film is indispensable to practical e-beam direct-writing. K-kit (Liu et al., 2008; Tai et al., 2012; Chen et al., 2014), a liquid sample holder, was utilized in this work for achieving such a uniform liquid thin film.

MATERIALS AND METHODS

A JEM-2010 JEOL transmission electron microscope (TEM) was utilized as an e-beam source. TEM provided a highly convergent and controllable e-beam and *in situ* and high-resolution imaging after the writing process. K-kit was used to confine the $CuSO_4$ solution in the high vacuum environment of the TEM and to allow the e-beam to pass through for observation. K-kit was composed of two silicon
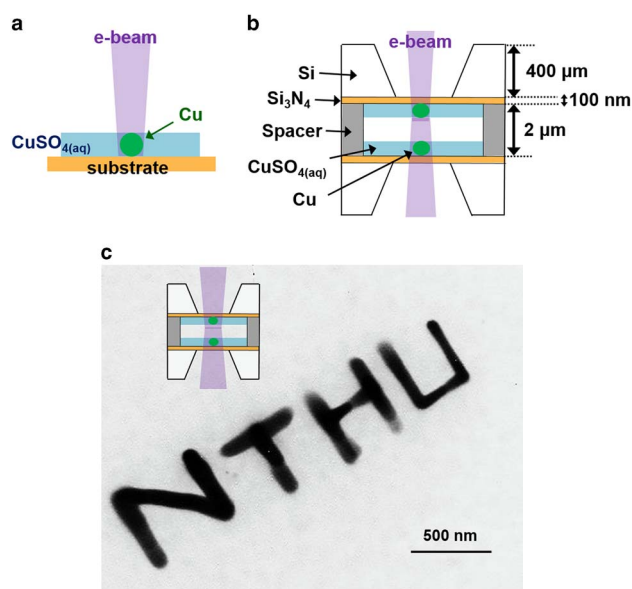
Figure 1. Reduction of Cu patterns from a thin $CuSO_4$ solution layer. **a:** Schematic diagram of reduction of Cu patterns from a thin $CuSO_4$ solution layer. **b:** Schematic diagram of K-kit used to demonstrate (**a**) in transmission electron microscopy (TEM) (the drawing is not to scale). **c:** TEM image of reduced Cu (this is a top-view image like the inset, only that on the upper layer is shown). The accelerating voltage was 200 kV. The e-beam with a beam current of 109 pA was converged to 50 nm in diameter and manipulated at 10 nm/s for reduction. Concentration of the $CuSO_4$ was 24 mM.

nitride films supported by silicon substrates that were bonded together with a spacer to form a $2\,\mu m$ sealed space, as shown in Figure 1b. K-kit was designed for one time use as the sample loading opening was sealed with glue after applying the solution. More geometric information about K-kit is shown in Supplementary Figure 1. Two layers of 24 mM $CuSO_4$ solution were then applied on the inner sides of both the upper and lower silicon nitride films employing a partial drying process (Liu, 2010). The e-beam was converged to 50 nm in diameter and moved at 10 nm/s along the designed path.

Supplementary Figure 1

Supplementary Figure 1 can be found online. Please visit journals.cambridge.org/jid_MAM.

RESULTS AND DISCUSSION

Direct-Writing of Cu Nano-Patterns

Figure 1c shows the direct-writing Cu nano-pattern NTHU, the abbreviation of the authors' institute. Because of the two-liquid-layer design of K-kit, two well-aligned Cu patterns were formed on the inside surfaces of the upper and lower silicon nitride films, respectively. Since Figure 1c was the top-view image, two patterns appeared as one. K-kit was then tilted to 30° in the TEM, and both of them were observed as shown in Supplementary Figure 3. The distance between the two layers of Cu patterns was 1,920 nm, which is consistent with the thickness of the spacer. More detail is discussed in the Supplementary Information "calculation of distance between two layers of Cu patterns." In applications like three-dimensional capacitance (Zhou et al., 2013), two well-aligned layers may be desired, which can be achieved by this process. In other applications like Cu interconnects, only one layer of a Cu pattern is desired and the $CuSO_4$ solution layer should be applied only on the substrate. The upper nitride film, serving as an e-beam window, should be hydrophobic and kept at a raised temperature (around 80–100°C) to avoid condensation. The thickness of each $CuSO_4$ solution layer was estimated to be 210 nm from an electron energy-loss spectrum (EELS). Thickness estimation is described in the Supplementary Information "calculation of thickness of $CuSO_4$ solution layer." Furthermore, the thickness of reduced Cu patterns was estimated to be 180–280 nm for the upper and 70–120 nm for the lower layer. There might have been some shadowing effect of the top Cu resulting in generally smaller Cu thickness on the lower layer. The thickness variation within each layer was attributed to the nonideal manual controlling of the writing sequence. If movement of the e-beam is controlled precisely, a Cu pattern with uniform thickness is possible. Details of the pattern thickness estimation is shown in Supplementary Figure 5 and discussed in "calculation of thickness of reduced Cu" in the Supplementary Information.

Supplementary Figures 3 and 5

Supplementary Figures 3 and 5 can be found online. Please visit journals.cambridge.org/jid_MAM.

Radiolysis of Water

The phenomenon of metal reduction from an ionic solution via an e-beam can be explained as a radiolysis process (Woehl et al., 2013; Grogan et al., 2014). The theory indicates that when water is irradiated by electrons with energy greater than the bond energy of valence electrons in the water (~10 eV), radical species and aqueous electrons are produced via ionization of water molecules. Products of the radiolysis process are: $H_2O \rightarrow e_{eq}^-$, $H^\bullet$, $OH^\bullet$, $HO_2^\bullet$, OH^-, H_3O^+, H_2, H_2O_2. Hydrogen radicals ($H^\bullet$), which is one kind of radical species, and aqueous electrons (e_{eq}^-) are expected to reduce metal ion. Metal reduced by an e-beam following the radiolysis process is also defined as electron beam-induced deposition (Donev & Hastings, 2009; Schardein et al., 2011; Ocola et al., 2012; Bresin et al., 2013).

In order to avoid the influence of gas phase radical species, two thin liquid layers of $CuSO_4$ solution were applied as described in the previous paragraph, leaving a gas phase in between the liquid layers. In effect, this creates a

thin liquid layer with liquid–gas interface right above the liquid. There are two major advantages of the thin liquid layers. First, the reduced Cu patterns were directly grown on the substrate surface. Second, the gas phase radical species readily escaped to the gas phase between the two liquid layers hindering bubble formation. Consequently, Cu patterns were static during repeated observations, even after 1 week. This positive result shows high potential in future industrial applications.

Influence Parameter on Cu Direct-Writing

To further understand this reaction, the influences of the concentration of the $CuSO_4$ solution and e-beam exposure time were studied. Since the energy required for radiolysis, the bond energy of water (~10 eV), is much smaller than typical e-beam sources (~100 keV), energy of an e-beam may not be a sensitive parameter. We then investigated how e-beam exposure time impacts reduced Cu, which may be helpful in selection of a suitable e-beam writing speed. Next, the side effects of higher or lower concentrations of $CuSO_4$ solution were demonstrated. Finally, the plot of Cu reduction rate versus concentration of $CuSO_4$ solution was obtained, and the reaction order was deduced.

E-Beam Exposure Time

To investigate the effect of e-beam exposure time on reduced Cu, a $CuSO_4$ solution was exposed to an e-beam for different times at different locations to generate a pseudo-time-lapse sequence of single dot writing. The TEM was operated at 200 kV, and an e-beam with a beam current of 109 pA was converged to 50 nm in diameter for reduction. Figure 2a shows eight dots formed by e-beam exposure with the exposure time of each dot indicated next to it. Concentration of the $CuSO_4$

solution was 24 mM. The mass of total Cu ion in K-kit and that in reduced dots was estimated to be 10^{-11} and 10^{-16} g, respectively. Diffusion was estimated to be in the milli-seconds range. It can be reasonably assumed that the initial condition for each dot writing was essentially identical. Therefore, the only variable for each dot was the e-beam exposure time. Generally, nucleation and grain growth is expected to be isotropic in three dimensions. However, in this case, the e-beam passed through in vertical direction. From Figure 2a, it can be seen that the lateral growth reached its saturation at 20 s, and the diameter was about 170 nm. We then calculated the thickness of each dot of the upper layer by the method mentioned above. TEM images of these eight dots after tilting K-kit 30° are shown in Supplementary Figure 6. Figure 2b shows the plot of thickness versus e-beam exposure time. The growth plot suggests there were basically two stages of growth in thickness. In stage 1, Cu was expected to nucleate homogeneously in the $CuSO_4$ solution. Therefore, tiny, loose Cu dots were formed in the beginning. The thickness appeared to increase rapidly, and the curve with large slope was obtained. In stage 2, the thickness growth rate was steady but slower, which means the thickness growth entered a different regime. It is worth noting that the solution thickness was estimated to be around 210 nm, which is comparable with the stage 1 thickness. We thus speculated that, during stage 1, Cu nucleation and grain growth was indeed isotropic in three dimensions in the liquid volume under e-beam illumination, while the Cu dots were small and density was low. The apparent thickness reached the liquid thickness rapidly. At later time, in stage 2, Cu nucleation increased and dots grew bigger, thickness increased only by the expansion of the packed Cu dots. One might observe that dots were thicker than the solution in stage 2. The possible reason is the formation of Cu dots was somewhat like volcanic island formation. New Cu
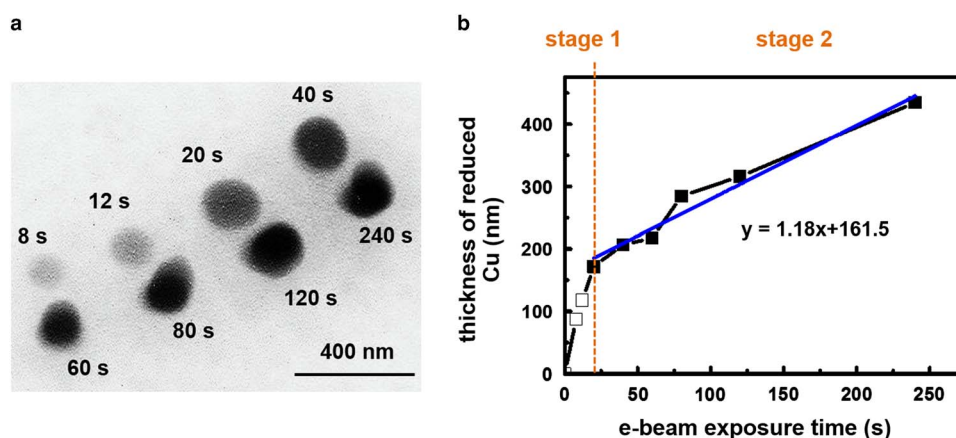

Figure 2. The analysis of different e-beam exposure time. **a:** Transmission electron microscope (TEM) image of Cu dots formed by e-beam exposure with the time indicated beside it. **b:** Plot of thickness of reduced Cu (upper layer) versus e-beam exposure time. There are two stages of the thickness growth rate. In stage 1 Cu nucleates homogeneously in $CuSO_4$, and loose Cu dots are formed. In stage 2, the growth rate of thickness is steady and slower, which means Cu dots grow bigger and are packed. The regression line of stage 2 is indicated beneath it. Accelerating voltage of the TEM was 200 kV, the e-beam with a beam current of 109 pA was converged to 50 nm in diameter for reduction, and the concentration of $CuSO_4$ was 24 mM.

was formed at the surface of Si_3N_4 and pushed the old Cu up to exceed the solution film. In any case, this plot may be useful in practical application to choose a suitable e-beam exposure time. For example, Cu interconnects require high electrical conductivity and dense Cu so that longer e-beam exposure time is needed. To increase throughput, multiple beam or pattern-projected e-beam illumination would be worth pursuing.

Supplementary Figure 6

Supplementary Figure 6 can be found online. Please visit journals.cambridge.org/jid_MAM.

Concentration of $CuSO_{4(aq)}$ Solution

Solution concentration was another important factor in the reaction. As shown in Figure 3, to demonstrate the impact of solution concentration on writing results, a Cu pattern was reduced in three different concentrations of $CuSO_4$ solution (2.4, 24, and 240 mM) with the same e-beam dosage. The TEM was operated at 200 kV. An e-beam with a beam current of 109 pA was converged to 50 nm in diameter and manipulated at 10 nm/s since continuous Cu patterns are usually desired. In Figure 3b, 24 mM seemed to be the most suitable concentration of $CuSO_4$ in this case. As shown in Figure 3a when the concentration was too low, some discontinuous lines formed. Based on results of the writing time study above, one might want to increase the e-beam exposure time or slow down the writing speed to form continuous lines. Figure 3c shows the side effect when the concentration was too high. There were many small particles about 30 nm in diameter freely nucleating in the background. This was mostly attributed to the Cu reduced during the imaging process while the solution was exposed to
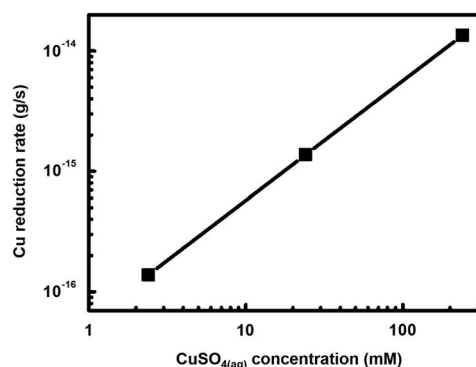
Figure 4. Plot of $CuSO_{4(aq)}$ concentration versus Cu reduction rate. Because of the linear correlation between $CuSO_{4(aq)}$ concentration and Cu reduction rate, it is a first order reaction with respect to Cu^{2+}.

an unconverged beam. Thus, it may be improved by diminishing the exposure time or e-beam dosage during the imaging process to avoid unwanted freely nucleating particles.

Cu Reduction Rate versus $CuSO_{4(aq)}$ Concentration

Finally, Figure 4 shows the reaction rate was directly proportional to the Cu^{2+} concentration. The data points were calculated from Figure 3. The horizontal axis of Figure 4 was the initial concentration of $CuSO_{4(aq)}$. The final concentration could not be detected because of evaporation of the solution during the loading and sealing process. However, due to the same amount of evaporation, the final concentration of these three samples was still exhibited a 10-fold difference between each other, which still made the reaction rate proportional to the Cu^{2+} concentration.
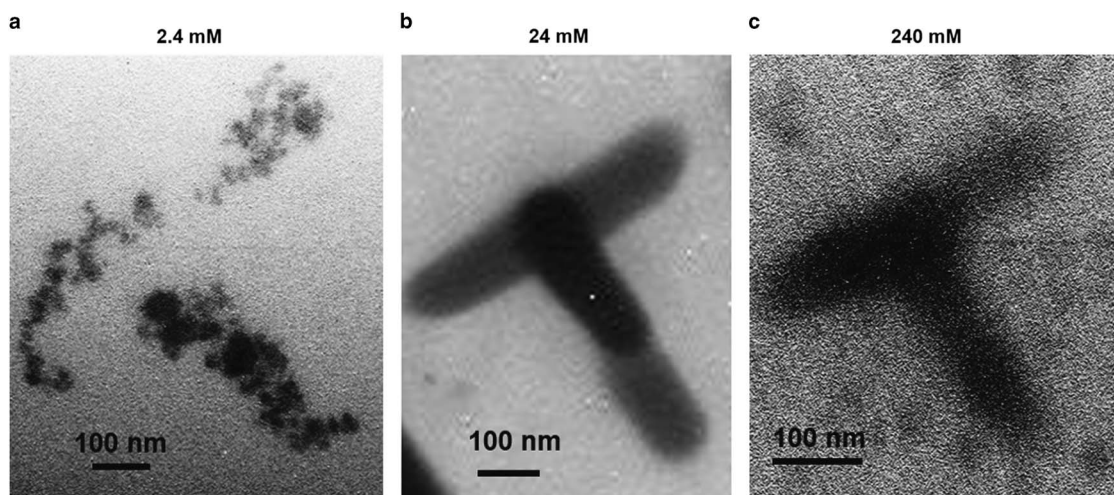
Figure 3. Transmission electron microscope (TEM) images of Cu reduced from different concentrations of $CuSO_{4(aq)}$. **a–c:** Concentrations of $CuSO_{4(aq)}$ are 2.4, 24, and 240 mM, respectively, as noted above each image. A continuous Cu line was formed in 24 mM. In, 2.4 mM, a discontinuous line was obtained. Some small particles about 30 nm in diameter freely nucleate in the 240 mM concentration. Accelerating voltage of the TEM was 200 kV. The e-beam with a beam current of 109 pA was converged to 50 nm in diameter and manipulated at 10 nm/s for reduction.

Conclusions

In general, in view of the importance of nano-scale Cu patterns, we have demonstrated a promising method to fabricate patterns. A uniform and stable liquid thin film, which facilitates Cu direct-writing, was created. The structure, a thin liquid layer of $CuSO_4$ solution on a substrate, was able to produce Cu patterns with a width finer than 100 nm by shifting the e-beam. Influences on the reduced Cu, including e-beam exposure time and concentration of the $CuSO_4$ solution, were discussed. The plots of thickness of reduced Cu versus e-beam exposure time and Cu reduction rate versus $CuSO_{4(aq)}$ concentration were obtained, which may be helpful in future applications. Finally, the Cu reduction rate was proportional to the Cu^{2+} concentration. In the future, finer Cu patterns are expected by applying an e-beam with a smaller convergent size or thinner $CuSO_4$ solution layer.

Acknowledgments

References

Bresin, M., Botman, A., Randolph, S.J., Straw, M. & Hastings, J.T. (2014). Liquid phase electron-beam-induced deposition on bulk substrates using environmental scanning electron microscopy. *Microsc Microanal* **20**(2), 376–384.

Bresin, M., Chamberlain, A., Donev, E.U., Samantaray, C.B., Schardien, G.S. & Hastings, J.T. (2013). Electron-beam-induced deposition of bimetallic nanostructures from bulk liquids. *Angew Chem* **52**(31), 8004–8007.

Chen, Y.T., Wang, C.Y., Hong, Y.J., Kang, Y.T., Lai, S.E., Chang, P. & Yew, T.R. (2014). Electron beam manipulation of gold nanoparticles. *RSC Adv* **4**, 31652–31656.

De, S., Higgins, T.M., Lyons, P.E., Doherty, E.M., Nirmalraj, P.N., Blau, W.J., Boland, J.J. & Coleman, J.N. (2009). Silver nanowire networks as flexible, transparent, conducting films extremely high DC to optical conductivity ratios. *ACS Nano* **3**(7), 1767–1774.

den Heijer, M., Shao, I., Radisic, A., Reuter, M.C. & Ross, F.M. (2014). Patterned electrochemical deposition of copper using an electron beam. *APL Mater* **2**(2), 022101.

Donev, E.U. & Hastings, J.T. (2009). Electron-beam-induced deposition of platinum from a liquid precursor. *Nano Lett* **9**(7), 2715–2718.

Friedli, V., Utke, I., Molhave, K. & Michler, J. (2009). Dose and energy dependence of mechanical properties of focused electron-beam-induced pillar deposits from $Cu(C_5HF_6O_2)_2$. *Nanotechnology* **20**(38), 385304.

Grogan, J.M., Schneider, N.M., Ross, F.M. & Bau, H.H. (2014). Bubble and pattern formation in liquid induced by an electron beam. *Nano Lett* **14**(1), 359–364.

Liu, K.L. (2010). Novel microchip (K-kit) for in-situ transmission electron microscopy of living organisms in aqueous conditions. Doctoral Thesis. National Tsing-Hua University.

Liu, K.L., Wu, C.C., Huang, Y.J., Peng, H.L., Chang, H.Y., Chang, P., Hsu, L. & Yew, T.R. (2008). Novel microchip for in situ TEM imaging of living organisms and bio-reactions in aqueous conditions. *Lab Chip* **8**(11), 1915–1921.

Manshina, A., Povolotskiy, A., Ivanova, T., Kurochkin, A., Tver'yanovich, Y., Kim, D., Kim, M. & Kwon, S.C. (2007). $CuCl_2$-based liquid electrolyte precursor for laser-induced metal deposition. *Laser Phys Lett* **4**(3), 242–246.

Ochiai, Y. (1996). Electron-beam-induced deposition of copper compound with low resistivity. *J Vac Sci Technol B* **14**(6), 3887–3891.

Ocola, L.E., Joshi-Imre, A., Kessel, C., Chen, B., Park, J., Gosztola, D. & Divan, R. (2012). Growth characterization of electron-beam-induced silver deposition from liquid precursor. *J Vac Sci Technol B* **30**(6), 06FF08.

Randolph, S.J., Botman, A. & Toth, M. (2013). Capsule-free fluid delivery and beam-induced electrodeposition in a scanning electron microscope. *RSC Adv* **3**(43), 20016–20023.

Schardein, G., Donev, E.U. & Hastings, J.T. (2011). Electron-beam-induced deposition of gold from aqueous solutions. *Nanotechnology* **22**, 015301.

Shelby, R.A., Smith, D.R. & Schultz, S. (2001). Experimental verification of a negative index of refraction. *Science* **292**(5514), 77–79.

Smith, D.R., Pendry, J.B. & Wiltshire, M.C. (2004). Metamaterials and negative refractive index. *Science* **305**(5685), 788–792.

Tai, L.A., Kang, Y.T., Chen, Y.C., Wang, Y.C., Wang, Y.J., Wu, Y.T., Liu, K.L., Wang, C.Y., Ko, Y.F., Chen, C.Y., Huang, N.C., Chen, J.K., Hsieh, Y.F., Yew, T.R. & Yang, C.S. (2012). Quantitative characterization of nanoparticles in blood by transmission electron microscopy with a window-type microchip nanopipet. *Anal Chem* **84**(15), 6312–6316.

Utke, I., Luisier, A., Hoffmann, P., Laub, D. & Buffat, P.A. (2002). Focused-electron-beam-induced deposition of freestanding three-dimensional nanostructures of pure coalesced copper crystals. *Appl Phys Lett* **81**(17), 3245–3247.

van de Groep, J., Spinelli, P. & Polman, A. (2012). Transparent conducting silver nanowire networks. *Nano Lett* **12**(6), 3138–3144.

Vazquez-Mena, O., Sannomiya, T., Villanueva, L.G., Voros, J. & Brugger, J. (2011). Metallic nanodot arrays by stencil lithography for plasmonic biosensing applications. *ACS Nano* **5**(2), 844–853.

Woehl, T.J., Jungjohann, K.L., Evans, J.E., Arslan, I., Ristenpart, W.D. & Browning, N.D. (2013). Experimental procedures to mitigate electron beam induced artifacts during in situ fluid imaging of nanomaterials. *Ultramicroscopy* **127**, 53–63.

Zhou, C., Zhang, Y., Li, Y. & Liu, J. (2013). Construction of high-capacitance 3D CoO@polypyrrole nanowire array electrode for aqueous asymmetric supercapacitor. *Nano Lett* **13**(5), 2078–2085.